ADVANCED PHOTONICS RESEARCH
Open Access
www.adpr-journal.com

Hydrogel Microlasers for Versatile Biomolecular Analysis Based on a Lasing Microarray

*Xuerui Gong, Zhen Qiao, Peng Guan, Shilun Feng, Zhiyi Yuan, Changjin Huang, Guo-En Chang, and Yu-Cheng Chen**

Biological microlasers, which utilize lasing emission as a sensing signal, have recently emerged as a promising approach in biotechnology. As such, biolasers with functionality are of great significance for the detection of tiny molecular interactions in biological systems. Despite the considerable progress achieved in biomaterial-based microlasers, the ability to manipulate nanoscale biostructures and functionalize molecules in microcavity represents a grand challenge. Herein, the development of hydrogel microlasers by exploiting the versatility and controllability of hydrogels is reported, where whispering-gallery-mode lasing is achieved by printing hydrogel droplets on a mirror. Lasing behaviors and fundamental characteristics of hydrogel lasers are explored under various water-monomer ratios and crosslinking degrees. Furthermore, a hydrogel lasing microarray is developed, providing a novel approach to study molecular interactions within the 3D hydrogel network structure. To demonstrate the potential application and functionality, Forster resonance energy transfer (FRET) peptide lasing is exploited for molecular analysis. Single-mode FRET laser emission is achieved by tuning the Forster distance in hydrogel droplets. Finally, different types of biomolecules are encapsulated to form biolasing. These findings not only highlight the ability of hydrogel biolasers for high-throughput biomolecular analysis but also provide deep insights into the relationship between biostructure and laser physics.

1. Introduction

Biological microlasers have advanced rapidly in recent years, demonstrating their immense potential to use lasing emission as a sensing signal for monitoring molecular interactions.[1–6] Such lasers are known for their distinct advantages in terms of signal amplification, narrow linewidth, and strong intensity, which lead to unprecedented detection sensitivity of tiny changes in biological systems.[7–11] Most biolasers were realized through the introduction of fluorescent biomolecules (gain) into millimeter-sized resonators, resulting in difficulties for further applications. As such, whispering-gallery-mode (WGM) microlasers have come into play for their high Q factor, low mode volume, and miniaturized size.[12–15] A plethora of biocompatible materials have been used to form microlasers in recent years, including proteins, poly(lactic acid), starch, lipids, liquid crystals, cellulose, and polymers.[13,16–26] To move a step forward, it is essential to realize microlasers with the versatility to design, control, and functionalize different biostructures and molecules within the cavity. Hydrogels, one of the most popular biomaterials, have received tremendous attention for its high versatility among biocompatible materials over decades.[27,28] Endowed with unique 3D network structures and a porous interface, hydrogels enjoy priority in a wide range of applications in drug delivery, therapeutics, tissue engineering, and biosensing devices.[29–31] Hydrogels can be used to encapsulate

X. Gong, Dr. Z. Qiao, Dr. S. Feng, Z. Yuan, Prof. Y.-C. Chen
School of Electrical and Electronics Engineering
Nanyang Technological University
50 Nanyang Ave., 639798, Singapore
E-mail: yucchen@ntu.edu.sg

P. Guan
School of Electronic Information and Electrical Engineering
Shanghai Jiao Tong University
Shanghai 200240, China

The ORCID identification number(s) for the author(s) of this article can be found under https://doi.org/10.1002/adpr.202000041.

DOI: 10.1002/adpr.202000041

Prof. C. Huang
School of Mechanical and Aerospace Engineering
Nanyang Technological University
50 Nanyang Ave., 639798, Singapore

Prof. C. Huang, Prof. Y.-C. Chen
School of Chemical and Biomedical Engineering
Nanyang Technological University
62 Nanyang Dr., 639798, Singapore

Prof. G.-E. Chang
Department of Mechanical Engineering, and Advanced Institute of Manufacturing with High-Tech Innovations
National Chung Cheng University
Chiayi 62102, Taiwan

biomolecules or cells because they provide the natural aqueous environment required for biomolecules to function in biological systems.[32] In particular, the degree of crosslinking can be tailored according to specific functionalities, such as the diffusion barrier, porous size, and interactions. Considering their good mechanical strength and modifiable chemical interactions, the stiffness of hydrogels can also be designed for engineering in cellular mechanics.[33,34] Hydrogel microarrays have also been implemented as a high-throughput platform for cellular and molecular screening.[35,36]

Inspired by the high versatility and controllability of hydrogels, this study aims to develop hydrogel microlasers and to explore their fundamental characteristics in biolasing. **Figure 1**a shows the concept of a hydrogel biolaser in which precursor solutions mixed with fluorescent dyes are printed on a highly reflective dielectric mirror to form a cap-like cavity. WGM laser emission was achieved through the optical confinement between the hydrogel droplet and the bottom mirror. Taking advantage of the unique physical properties of the hydrogel, lasing behaviors could be fully manipulated by different degrees of polymerization and monomer ratios. The obtained laser signal was found to be closely related to the structural transformation in hydrogel cavities. Furthermore, a hydrogel lasing microarray was developed through inkjet printing, contributing a novel platform to study molecular interactions within 3D hydrogel network structures. Figure 1b shows the photo and fluorescence image of a hydrogel microarray after UV curing. Various droplet sizes, volumes, and fluorophores could be fabricated by programming the inkjet printer (Figure S1, Supporting Information), where the smallest laser diameter that could be achieved was 20 μm (Figure S2, Supporting Information).

To demonstrate potential applications and the functionality of the hydrogel laser array, Forster resonance energy transfer (FRET)-based detection was introduced in the hydrogel by exploiting fluorescent-peptide conjugates. Molecular distances between FRET pairs could be adjusted by different polymerization degrees, resulting in different FRET lasing intensities. Single-mode laser emission was achieved with a significantly increased FRET lasing intensity, suggesting a sensitive platform for monitoring biomolecular interactions. Finally, to manifest the versatility of hydrogel microlasers, peptides with diverse molecular weights were encapsulated to form biolasing. The lasing spectra and thresholds generated from fluorescent peptides revealed the role of molecular size in lasing performance. Our results not only provide deep insights into the relationship between biostructure and lasing properties but also mark a critical step toward using hydrogel lasers in high-throughput molecular analysis.

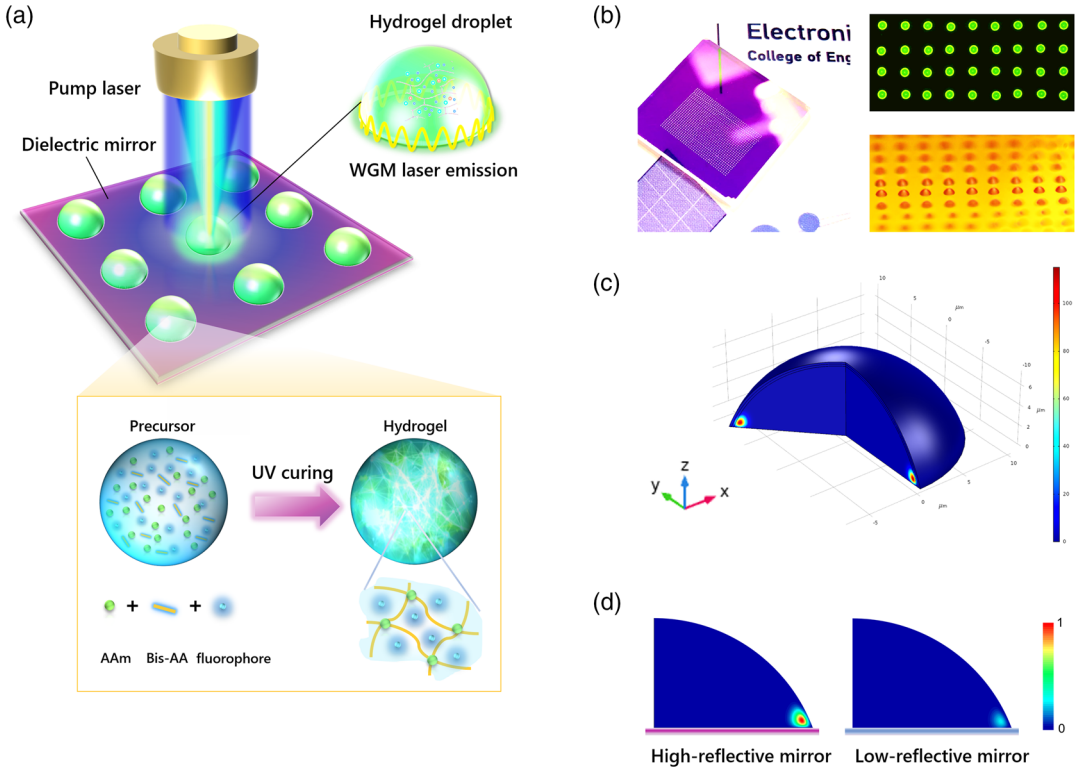

Figure 1. a) Schematic diagram showing the concept of hydrogel biolasers and hydrogel lasing microarray, which is supported by WGM. The bottom inset shows a transformation of hydrogel inner structure after UV curing. Fluorophores confined inside the polymer network form the gain medium of the hydrogel laser. b) The photograph of a hydrogel microarray printed on a dielectric mirror. Right panel: fluorescent image of hydrogel array excited by LED pump (top). All the droplets in this image present a diameter of 20 μm, which is the minimum size that can be achieved. An enlarged microscopic image of the hydrogel array (bottom). c) Simulated 3D electric field distribution of a WGM droplet resonator placed on the mirror (diameter of 20 μm). d) Comparison of the WGMs when a microdroplet is placed on a high reflective mirror (Q factor $= 7 \times 10^4$) and a low reflective mirror (Q factor $= 2.0 \times 10^2$).

2. Results and Discussion

2.1. Investigation of Lasing Behaviors in Hydrogel Array

To explore the possibility of obtaining lasing with a water-based microcavity, the lasing modes of a hydrogel droplet resonator were first simulated based on a 20 μm sized hydrogel droplet. Figure 1c shows the typical WGM, which resonates around the bottom of a droplet. To understand the mechanism of the mirror underneath, we compared the Q factors and electric field strengths of WGMs under high- and low-reflectivity mirrors in Figure 1d. Under a high-reflectivity mirror ($R > 99\%$), the WGM possesses a reasonably high Q factor (7×10^4) and strong electric field strength. When the bottom mirror has the same resonant wavelength as the gain in a droplet, the overall threshold becomes lower; therefore, more laser modes and higher intensity are expected. On the contrary, the Q factor (2×10^2) becomes two orders of magnitude lower when the bottom substrate possesses a low-reflectivity mirror ($R < 1\%$), resulting in lower electric field strength and lower number of laser modes. Herein, the tremendous difference in the Q factor illustrates the critical role of the bottom mirror for achieving lasing conditions in a hydrogel droplet resonator.

As a first step, hemisphere microdroplets were printed on a highly reflective dielectric mirror by using water/glycerol (volume ratio 1:1) to form the cavity and fluorescein isothiocyanate (FITC) as the gain material. In comparison to previous works that used high-precision dispensers to fabricate microlasers,[37,38] it is noteworthy that here we only modified an office inkjet printer to achieve microlaser arrays (Figure S1, Supporting Information). WGM laser emissions were obtained and verified by the free spectral range corresponding to the droplet diameter (Figure S3a, Supporting Information). Such lasing emissions are quite stable and can lase for up to 1 min, as shown in the video (Supporting Information). Taking advantage of the versatility of the inkjet printer, the lasing wavelength could be adjusted by changing different fluorophores. For instance, lasing from rhodamine-B (RhB) was observed around 610 nm (Figure S3b, Supporting Information) with a threshold of 3.6 μJ mm^{-2} (Figure S3c, Supporting Information). The diameter of droplet microlaser (20–100 μm) or contact angle could be adjusted by programming the inkjet printer. We also demonstrated lasing with proteins (Figure S3d, Supporting Information), suggesting that any type of water-based biological agent could be printed to form a lasing microarray.

Moving forward, we attempted to implement the same approach to achieve hydrogel lasers. By replacing glycerol with an acrylamide (AAm) monomer and crosslinkers, hydrogel precursors mixed with FITC or RhB were printed on mirror. Laser emissions from hydrogels were observed, as shown in **Figure 2**a,b, respectively. The free spectral range corresponds well with the hydrogel droplet diameter, following the basic principle of the WGM. It is noteworthy that no 3D network structure was formed inside the cavity before polymerization. However, complex 3D networks are formed after the polymerization reaction. To investigate how such a 3D network structure will make an impact on the lasing behavior, we compared the lasing performance by adjusting the monomer/water ratio from 10% to 50% under a fixed pump intensity in Figure 2c. To our surprise, the lasing intensity increased significantly with the increment of monomer ratios (Figure 2d,e). This interesting result shows that the lasing behavior of hydrogels is highly dependent on the inner structure of hydrogels, which can be attributed to the difference in terms of refractive indexes. The higher the monomer ratio, the higher is the refractive index, which will lead to a higher Q factor and thus lasing intensity.

On the other hand, we investigated how polymerization (degree of crosslinking) may affect the lasing behavior, based on a fixed content (monomer/water ratio). The differences can also be clearly seen in laser modes, before and after polymerization, in Figure 2f. Apparently, several ring modes were formed inside the hydrogel after polymerization (bottom photo). Numerous higher-order modes were observed as well, which are likely the result of the 3D network structure formed inside the hydrogel. Furthermore, we measured the lasing threshold of the precursor and polymerized hydrogel. The lasing spectra of the hydrogel under various pump energy densities are plotted in Figure 2g. Figure 2h shows the spectrally integrated laser output as a function of pump energy density (610–630 nm) extracted from Figure 2g. A lower lasing threshold was found for the polymerized hydrogel as a result of a slightly increased refractive index. However, the increased value of the refractive index was not very obvious and thus did not become a dominating factor, which is consistent with a previous report.[39]

2.2. Hydrogel Lasing Controlled by Molecular Interactions

On the basis of the hydrogel laser, we aim to investigate how such microlasers could be applied in biomolecular analysis. Herein, we introduced FRET pairs in hydrogels (Figure S4, Supporting Information) to demonstrate how the FRET lasing efficiency can be modulated by tuning the Forster distance in hydrogel microdroplets (**Figure 3**a and Figure S5, Supporting Information). By changing the amount of the photoinitiator, the polymerization degree will influence the FRET lasing performance. Figure 3b first shows the lasing spectrum of the FRET laser resulted from pure FITC–RhB. To monitor the interaction between molecules, two peptides, including Gly-His and L-glutathione oxidized (GSH), were selected to conjugate with an FITC *N*-hydroxysuccinimide ester (FITC-NHS) and a rhodamine *N*-hydroxysuccinimide ester (RhB-NHS) respectively. Figure 3c shows the lasing spectrum obtained from the hydrogel containing FITC-Gly-His and RhB-GSH dye–peptide conjugates, where FRET-peptide lasing was achieved. To our surprise, the FRET emission signals received were nearly single-mode rather than multimode lasing. We further explored the cause of this interesting phenomenon using theoretical calculation and provided two explanations: 1) different lasing threshold conditions caused by intrinsic optical property of RhB molecules and 2) different Q factors of the hydrogel cavity resulting from the different reflectivity of the bottom mirror substrate. The first point can be understood by the required population inversion for RhB dye molecules. Considering the Q factor and dye concentration used, the lasing threshold for RhB was found to be relatively low, around 623 nm, which enabled the WGM mode to reach lasing easier than other wavelengths. Detailed calculation can be found in Figure S6 and S7, Supporting Information. The second point

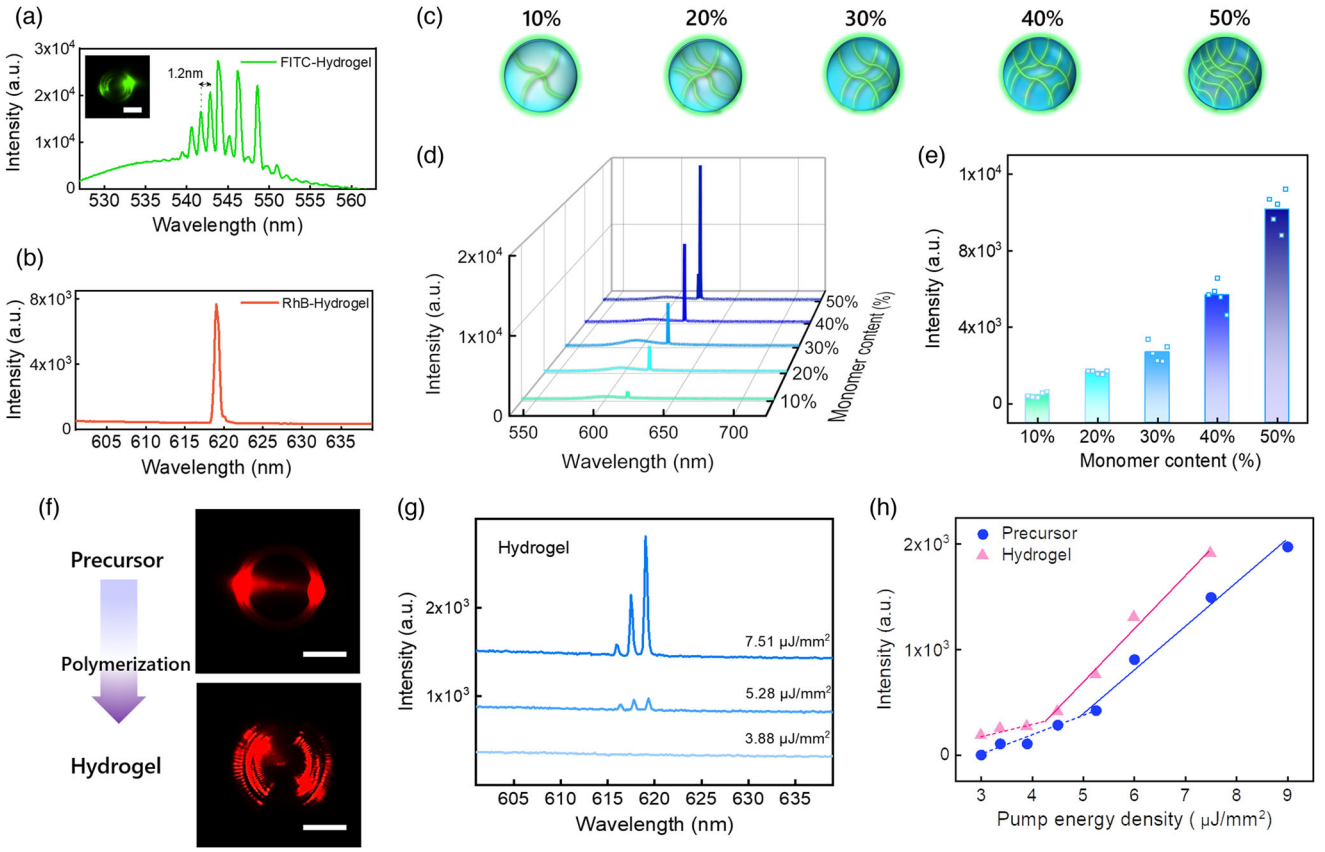

Figure 2. a,b) Lasing spectra obtained from hydrogel microlaser by mixing precursor with (a) 2 mM FITC and b) 2 mM RhB, respectively. The inset shows the laser mode image from one hydrogel droplet. The excitation wavelength for FITC was 480 nm and for RhB 530 nm. c) The schematic diagram shows the difference of the inner hydrogel structure with different monomer/water ratios (%) in the precursor. d) Lasing spectra obtained from hydrogel droplet with different monomer content ratios and the same diameter of 60 μm. The encapsulated RhB concentration was 2 mM. Pump energy density = 57 μJ mm^{-2} for all collected spectra. e) The lasing intensity distribution extracted from (d). f) Comparison of the laser mode obtained from the precursor and hydrogel (before and after polymerization). g) Lasing spectra of the hydrogel containing 2 mM RhB under different pump energy densities; the curves have been shifted for clarity. h) Comparison of lasing threshold between the precursor and polymerized hydrogel. Scale bars, 30 μm. Curing time = 5 s.

can be explained by the effective Q factor of the hydrogel cavity at the respective wavelengths, depending on the reflectivity of the bottom mirror. Figure S8, Supporting Information, shows the calculated Q factor of the hydrogel cavity with a low reflective mirror and high reflective mirror from 615 to 630 nm. Due to the mirror's low reflectivity around the RhB emission wavelength, the radiative Q factor was constricted and decreased compared to that with a high reflective mirror. Nonetheless, according to calculation results, only the Q factor of the WGM at 620 nm was still higher than the threshold Q factor, thus enabling it to compensate for the losses, forming a sharp single mode on the spectrum.

With a fixed control of molecule concentrations and UV curing time, an increased amount of photoinitiator will lead to a higher degree of polymerization. FRET pairs would be squeezed by a smaller interval than those with a lower polymerization degree, resulting in higher energy transfer efficiency (Figure 3a). Consequently, the distance between the donor molecules and acceptor molecules could be adjusted by a polymerization degree (crosslinking degree). We first chose three photoinitiator concentrations (0, 20, and 45 mg) as a comparison to study how the polymerization degree may influence the FRET lasing performance. Figure S9a, S9b, Supporting Information, shows the lasing threshold curves for FRET lasing with different photoinitiator concentrations. Only a slight difference could be distinguished, indicating the change of Forster distance could not be entirely reflected by lasing thresholds. Theoretical calculations were also performed by considering the respective FRET efficiency and Foster distances (Figure S9c, Supporting Information), which were in good agreement with the experiment's results. However, the calculation results suggested a significant trend in terms of lasing intensity near the threshold, which may be an alternative parameter to quantify FRET interactions.

Herein, we used the lasing intensity, as shown in Figure 3d,e, to show the controllability of molecular interactions and lasing action by adjusting the photoinitiator concentration in hydrogels. The pump energy density was selected based on the threshold of 0 mg lasing threshold. We first tested hydrogel lasers with FITC-RhB fluorophores in Figure 3d. Under a fixed UV curing time, the integrated FRET laser intensity increased linearly,

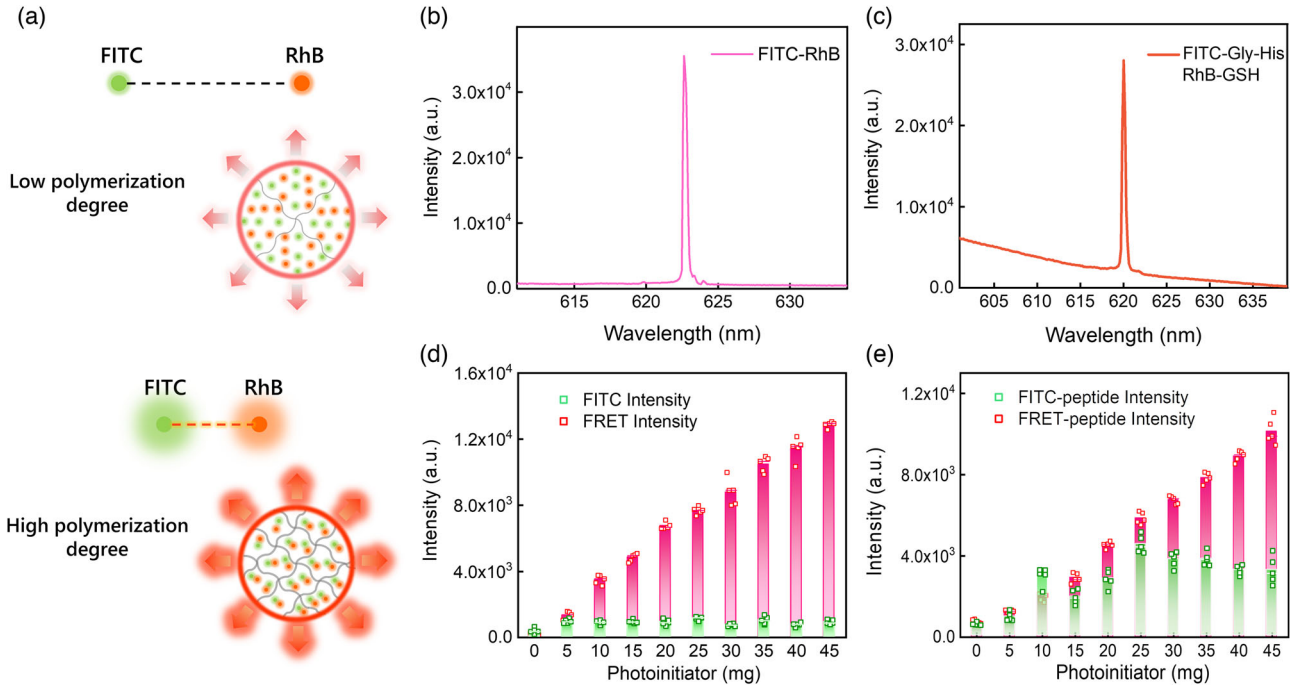

Figure 3. a) Schematic diagram showing FRET interaction in hydrogel microdroplet with low polymerization degree and high polymerization degree. FRET is formed by 2 mM RhB and 2 mM FITC. The Foster distances become smaller at a higher polymerization degree. b,c) Lasing spectra obtained from hydrogel containing (b) 2 mM FITC-RhB FRET pairs and (c) 2 mM FITC-Gly-His/RhB-GSH pairs. d) Comparison between the integrated intensity of laser output obtained from the hydrogel containing pure FITC and FRET pairs, under various photoinitiator concentrations. e) Comparison between the integrated intensity of laser output obtained from FITC-Gly-His and FRET-peptide pairs, under various photoinitiator concentrations. UV curing time = 5 s. All droplet diameter = 60 μm. Pump energy density = 75 μJ mm^{-2}. Excitation wavelength = 480 nm.

reflecting a higher FRET efficiency (pink bars). Similar results were obtained by using FRET peptide pairs (FITC-*Gly-His* and RhB-*GSH*) in Figure 3e (pink bars). As a control group, the lasing intensity of hydrogel lasers without FRET pairs (only FITC or FITC-*Gly-His*) is shown in Figure 3d,e, respectively (green bars). Figure 3d shows that lasing intensity only increased between 0 and 5 mg, while the intensity remained beyond 5 mg. In Figure 3e, the lasing intensity increased between 0 and 25 mg and started to drop gradually. In contrast, the FRET-peptide laser intensity (pink bars) increased significantly when the photoinitiator reached above 25 mg. To confirm that the increase of FRET laser intensity can be attributed to the increased FRET efficiency, the corresponding fluorescence spectra are provided in Figure S4, Supporting Information.

2.3. Hydrogel Lasing with Different Biomolecules

Finally, to demonstrate the wide applicability of the hydrogel lasing microarray, different types of biomolecules were selected based on molecular weights. **Figure 4**a shows a schematic diagram of the three biomolecules conjugated to RhB-NHS, including insulin (5734 g mol^{-1}), V5-peptide (1524 g mol^{-1}), and GSH (612 g mol^{-1}). As a control group, RhB-NHS was plotted and analyzed. All four fluorophore conjugates were mixed with hydrogel monomers and printed to from lasing microarrays. Figure 4b–e shows the respective lasing spectra obtained from the hydrogel array with RhB-insulin, RhB-V5, RhB-GSH, and pure RhB-NHS, respectively. In addition to the lasing spectrum, Figure 4f shows the spectrally integrated laser output as a function of the pump energy density.

From our results in Figure 4f, we found that when RhB-NHS binds to biomolecules, the lasing threshold tends to become smaller. Given that there seems to be a trend between the lasing threshold and the encapsulated molecular size, many factors should be considered. Here we provided two possible explanations. First, the introduction of larger molecules increased the Rayleigh scattering in the whole system. Studies have reported that scattering can serve as a decisive factor for enhanced lasing in the WGM cavity.[40] With more substantial scattering, the light path inside the cavity will be longer, which in turn elongates the photon lifetime inside the cavity. The mentioned three molecules could have a similar effect inside the hydrogel cavity, resulting in a lower lasing threshold. To be more specific, we calculated the corresponding fraction of scattered light, as discussed in the Supporting Information.[41,42] With the Rayleigh scattering cross-section and the corresponding molecular number, the fraction of light scattered by the respective molecules was 2×10^{-2} for insulin, 6.02×10^{-4} for V5, and 2.04×10^{-4} for GSH; therefore, larger molecules may generate stronger lasing emissions. Second, larger molecules have more tendency to adhere to the interface, particularly the interface between the mirror and droplet. Consequently, more gain will contribute to the WGM lasing, thus generating a lower lasing threshold. Finally, we explored the detection limit of the hydrogel microlasers, as shown in

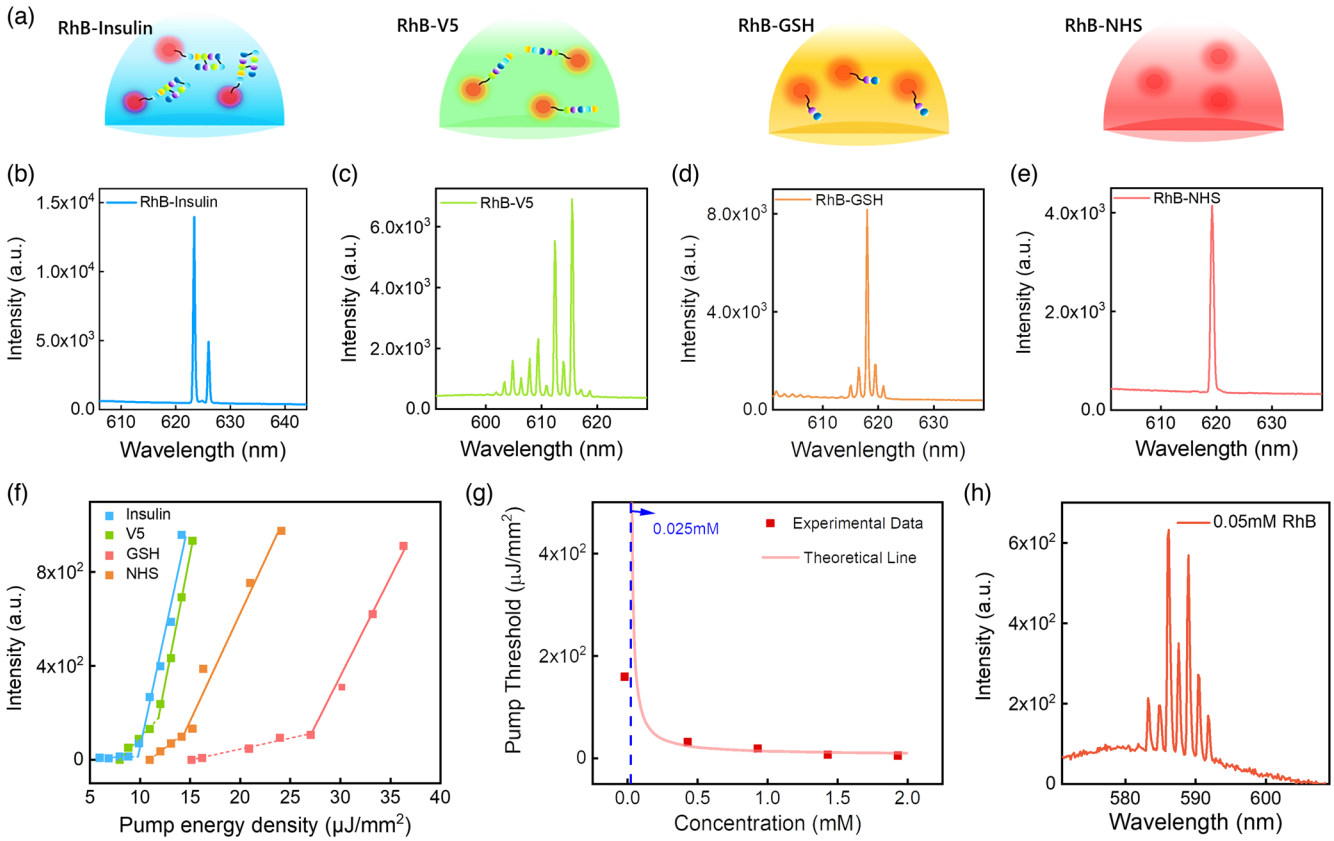

Figure 4. a) Schematic diagram of biological molecules encapsulated by hydrogel droplets where RhB was used for fluorophore conjugation. b–e) Lasing spectra obtained from the hydrogel containing (b) RhB-insulin (5734 g mol^{-1}), (c) RhB-V5 (1524 g mol^{-1}), (d) RhB-GSH (612 g mol^{-1}), and (e) RhB-NHS above their respective lasing thresholds. The concentration of RhB-NHS was fixed at 2 mM for all samples. The excitation wavelength for all the droplets ($D = 60$ μm) was fixed at 530 nm. f) Spectrally integrated laser output obtained from hydrogel containing different RhB–peptide conjugates as a function of pump energy density. g) Lasing threshold for hydrogel encapsulated with different RhB concentrations. The lowest presented concentration here is 0.05 mM. The solid dots represent experimental data and the pink curve represents the theoretical fitting. h) Lasing spectrum obtained from hydrogel containing 0.05 mM RhB fluorophore.

Figure 4g. The concentration of RhB was adjusted in the hydrogel array to study the threshold required for lasing. The lowest concentration to obtain a stable lasing signal in the hydrogel was ≈50 μM (Figure 4h), which is an acceptable range for bioanalysis. We also used rate equations in the Supporting Information (Equation 3,4) to better illustrate the relations between the lasing threshold and RhB concentration, as shown by the pink curve in Figure 4g. Herein the expected detection limit for lasing is close to 25 μM, implying that it is possible to detect a biomolecule or agent of this order.

3. Conclusion

In this study, we developed a fully functional, controllable, and biocompatible microlaser by using hydrogels. The realization of a hydrogel laser marks a critical step for using hydrogel lasers in a wide range of biomedical applications. As such, various biomolecules and fluorophores could be encapsulated within the hydrogel to form lasing at desirable wavelengths. Fundamental lasing properties of hydrogel lasers were explored under different water–monomer ratios and degrees of polymerization. Our results revealed that the internal 3D hydrogel networks and biological structures would have a significant impact on their lasing output, including thresholds, lasing modes, and spectra. In addition, a hydrogel lasing microarray was demonstrated by inkjet printing. To the best of our knowledge, this is the first microlaser array that can be easily fabricated on-chip by an office printer. Finally, single-mode FRET lasing was manipulated through biomolecular interactions, paving a new way for high-throughput biomedical analysis.

4. Experimental Section

Materials: The dyes used in this study were fluorescein sodium salt (Sigma-Aldrich #F6377), rhodamine B (Tokyo Chemical #A5102), 5(6)-carboxyfluorescein *N*-hydroxysuccinimide ester (Sigma-Aldrich #21878), and NHS-rhodamine (Thermal Fisher Scientific #46406). For the hydrogel, AAm (Sigma Aldrich #A9099) was selected as the monomer, *N*, *N*′-methylenebis(acrylamide) (Sigma #146072) as the crosslinker to form the 3D structure, and 2-hydroxy-4′-(2-hydroxyethoxy)-2-methylpropiophenone (Sigma # 410896) as the photoinitiator to trigger polymerization. To prepare dye–peptide conjugates, Gly-His (Sigma Aldrich #G1627),

L-glutathione oxidized (Sigma Aldrich #G4376), V5 peptide (Sigma Aldrich #V7754), insulin (Sigma Aldrich #I6634), and protein standard (BSA, 200 mg ml^{-1}) (Supelco #P5369) were used as bioagents to combine with the NHS ester.

Array Fabrication: For the water-based array, 0.8 mg FITC was added into a 1 mL mixture of water and glycerol (volume ratio 1:1) and then mixed on the vortex. The final dye concentration was 2 mM. Then the solution was added into the printer and printed on a dielectric mirror. For the hydrogel-based array, 0.475 g AAm and 0.025 g *N*,*N*′-methylenebis(acrylamide) (bis-AA) were dissolved in 500 µL deionized water to prepare the precursor solution. Furthermore, 35 mg photoinitiator was added into the solution to trigger polymerization after UV curing (Panasonic #ANUJ3500). Then 0.8 mg FITC/1 mg RhB was added into the precursor. The final dye concentration was 2 mM. The prepared precursor was added into the printer and printed on a dielectric mirror (customized by Evaporation Coatings Inc, USA). At last, the printed array was illuminated by a UV curing system for 5 s.

FRET Pair Preparation: For FITC-RhB pairs, 0.8 mg FITC and 1 mg RhB were added into the precursor solution and then mixed on the vortex. Final concentrations of FITC and RhB were both 2 mM.

For FITC-Gly-His conjugates, 1 mg FITC-NHS was first dissolved in 25 µL *N*,*N*-dimethylformamide (DMF). In 200 µL triethylammonium bicarbonate buffer (Sigma Aldrich #T7408), 0.6 mg Gly-His was dissolved. Then, the two solutions were mixed and reacted under room temperature for 2 h. For RhB-GSH conjugates, 1.1 mg RhB-NHS was dissolved in 25 µL DMF, and 1.3 mg of GSH was dissolved in 200 µL PBS buffer. Then, the two solutions were mixed and reacted under room temperature for 2 h. After the reaction, the prepared conjugates were mixed, and 100 µL ethanol was added into the solution. The final concentration of dyes was 2 mM, and the peptides were prepared excessively to ensure all fluorophores had been conjugated with peptides. Then 0.475 g AAm and 0.025 g bis-AA were added and dissolved on the vortex. Finally, different amounts of the photoinitiator were added into the prepared solution, ranging from 0 to 45 mg.

Preparation of Dye–Peptide Conjugates: First, 1.6 mg RhB-NHS was dissolved in 50 µL DMF. Then, 1.3 mg GSH, 1.5 mg V5-peptide, and 5 mg insulin were dissolved in 350 µL PBS buffer, separately. Later, RhB-NHS solution was added into each group and reacted with the bioagents under room temperature for 2 h. RhB-NHS solution was also added into 350 µL PBS buffer as a comparison group. After reaction, 0.475 g AAm, 0.025 g bis-AA, and 35 mg photoinitiator were added into the prepared solution and dissolved on the vortex. Finally, 100 µL ethanol was added to the solution. The final concentration of RhB in every group was 2 mM and all the peptides were prepared excessively to ensure that RhB-NHS was totally conjugated.

Optical System Setup: A microscopic system (Nikon Ni2) with 10× 0.3 NA objective was used to pump the hydrogel array and collect light. Optical pumping was achieved by a pulsed nanosecond laser (EKSPLA PS8001DR) integrated with an optical parametric oscillator with a repetition rate of 50 Hz and pulse duration of 5 ns. According to the respective absorption wavelengths of fluorophores, the pump laser was tuned to 488 nm for FITC and FRET or 532 nm for RhB. The beam diameter at the objective focal plane was ≈40 µm. The collected light was transmitted to a charge-coupled device camera or an imaging spectrometer (Andor Kymera 328i and Newton 970 EMCCD). For measurements of the fluorescence image, an integrated light-emitting diode (LED) was used as the excitation source and imaged by a CCD (Andor Zyla SCMOS) mounted on the microscope.

Supporting Information

Supporting Information is available from the Wiley Online Library or from the author.

Acknowledgements

X.G. and Z.Q. contributed equally to this work. The authors are thankful for the lab support from the Centre of Bio-Devices and Signal Analysis and Internal Grant NAP SUG – M4082308.040 from the Nanyang Technological University. The authors are also thankful for the financial support from Agency for Science, Technology and Research (A*STAR) (No. A2084c0063).

Conflict of Interest

The authors declare no conflict of interest.

Keywords

biomolecular analysis, hydrogels, microarrays, microlasers, whispering-gallery mode

Received: August 19, 2020
Published online:

[1] Y. C. Chen, X. Fan, *Adv. Opt. Mater.* **2019**, *7*, 1900377.
[2] J. E. Hales, G. Matmon, P. A. Dalby, J. M. Ward, G. Aeppli, *Nat. Commun.* **2019**, *10*, s41467-019-11604-z.
[3] Y.-C. Chen, Q. Chen, X. Fan, *Optica* **2016**, *3*, 809.
[4] X. Fan, S.-H. Yun, *Nat. Methods* **2014**, *11*, 141.
[5] Y.-C. Chen, X. Tan, Q. Sun, Q. Chen, W. Wang, X. Fan, *Nat. Biomed. Eng.* **2017**, *1*, 724.
[6] Q. Chen, X. Zhang, Y. Sun, M. Ritt, S. Sivaramakrishnan, X. Fan, *Lab Chip* **2013**, *13*, 2679.
[7] M. Schubert, L. Woolfson, I. R. M. Barnard, A. Morton, B. Casement, G. B. Robertson, G. B. Miles, S. J. Pitt, C. S. Tucker, M. C. Gather, *Nat. Photonics* **2020**, *14*, 452.
[8] X. Yang, W. Shu, Y. Wang, Y. Gong, C. Gong, Q. Chen, X. Tan, G.-D. Peng, X. Fan, Y.-J. Rao, *Biosens. Bioelectron.* **2019**, *131*, 60.
[9] S. Caixeiro, M. Gaio, B. Marelli, F. G. Omenetto, R. Sapienza, *Adv. Opt. Mater.* **2016**, *4*, 998.
[10] W. Lee, Q. Chen, X. Fan, D. K. Yoon, *Lab Chip* **2016**, *16*, 4770.
[11] M. C. Gather, S. H. Yun, *Nat. Photon.* **2011**, *5*, 406.
[12] Z. Yuan, Z. Wang, P. Guan, X. Wu, Y. C. Chen, *Adv. Opt. Mater.* **2020**, *8*, 1901596.
[13] V. D. Ta, Y. Wang, H. Sun, *Adv. Opt. Mater.* **2019**, *7*, 1900057.
[14] A. Fernandez-Bravo, K. Yao, E. S. Barnard, N. J. Borys, E. S. Levy, B. Tian, C. A. Tajon, L. Moretti, M. V. Altoe, S. Aloni, *Nat. Nanotechnol.* **2018**, *13*, 572.
[15] A. H. Fikouras, M. Schubert, M. Karl, J. D. Kumar, S. J. Powis, A. di Falco, M. C. Gather, *Nat. Commun.* **2018**, *9*, 4817.
[16] V. D. Ta, S. Caixeiro, F. M. Fernandes, R. Sapienza, *Adv. Opt. Mater.* **2017**, *5*, 1601022.
[17] T. Van Nguyen, N. Van Pham, H. H. Mai, D. C. Duong, H. H. Le, R. Sapienza, V.-D. Ta, *Soft Matter* **2019**, *15*, 9721.
[18] Y. Wei, X. Lin, C. Wei, W. Zhang, Y. Yan, Y. S. Zhao, *ACS Nano* **2017**, *11*, 597.
[19] M. Humar, A. Dobravec, X. Zhao, S. H. Yun, *Optica* **2017**, *4*, 1080.
[20] L. Zhao, Y. Wang, Y. Yuan, Y. Liu, S. Liu, W. Sun, J. Yang, H. Li, *Opt. Commun.* **2017**, *402*, 181.
[21] A. Jonáš, M. Aas, Y. Karadag, S. Manioğlu, S. Anand, D. McGloin, H. Bayraktarc, A. Kiraz, *Lab Chip* **2014**, *14*, 3093.
[22] X. Li, Y. Qin, X. Tan, Y.-C. Chen, Q. Chen, W.-H. Weng, X. Wang, X. Fan, *ACS Photon.* **2019**, *6*, 531.
[23] Z. Lv, Z. Man, Z. Xu, C. Feng, Y. Yang, Q. Liao, X. Wang, L. Zheng, H. Fu, *ACS Appl. Mater. Interfaces* **2018**, *10*, 32981.
[24] G. Pirnat, M. Humar, I. Muševič, *Opt. Exp.* **2018**, *26*, 22615.

[25] Z. Gao, W. Zhang, Y. Yan, J. Yi, H. Dong, K. Wang, J. Yao, Y. S. Zhao, *ACS Nano* **2018**, *12*, 5734.
[26] Y. Wang, L. Zhao, A. Xu, L. Wang, L. Zhang, S. Liu, Y. Liu, H. Li, *Sens. Actuators, B* **2018**, *258*, 1090.
[27] H.-I. Park, S.-Y. Park, *ACS Appl. Mater. Interfaces* **2018**, *10*, 30172.
[28] A. Matsumoto, M. Tanaka, H. Matsumoto, K. Ochi, Y. Moro-Oka, H. Kuwata, H. Yamada, I. Shirakawa, T. Miyazawa, H. Ishii, *Sci. Adv* **2017**, *3*, eaaq0723.
[29] K. Y. Lee, D. J. Mooney, *Chem. Rev* **2001**, *101*, 1869.
[30] J. Li, D. J. Mooney, *Nat. Rev. Mater.* **2016**, *1*, 1.
[31] L. Li, Y. Wang, L. Pan, Y. Shi, W. Cheng, Y. Shi, G. Yu, *Nano Lett.* **2015**, *15*, 1146.
[32] V. H. Pérez-Luna, O. González-Reynoso, *Gels* **2018**, *4*, 61.
[33] W. Lee, N. Kalashnikov, S. Mok, R. Halaoui, E. Kuzmin, A. J. Putnam, S. Takayama, M. Park, L. McCaffrey, R. Zhao, *Nat. Commun.* **2019**, *10*, 1.
[34] M. Dolega, M. Delarue, F. Ingremeau, J. Prost, A. Delon, G. Cappello, *Nat. Commun.* **2017**, *8*, 1.
[35] L. Jongpaiboonkit, W. J. King, G. E. Lyons, A. L. Paguirigan, J. W. Warrick, D. J. Beebe, W. L. Murphy, *Biomaterials* **2008**, *29*, 3346.
[36] P. Gagni, A. Romanato, G. Bergamaschi, P. Bettotti, R. Vanna, C. Piotto, C. F. Morasso, M. Chiari, M. Cretich, A. Gori, *Nanoscale Adv.* **2019**, *1*, 490.
[37] J. Zhao, Y. Yan, Z. Gao, Y. Du, H. Dong, J. Yao, Y. S. Zhao, *Nat. Commun.* **2019**, *10*, 1.
[38] V. D. Ta, S. Yang, Y. Wang, Y. Gao, T. He, R. Chen, H. V. Demir, H. Sun, *Appl. Phys. Lett.* **2015**, *107*, 221103.
[39] M. Choi, M. Humar, S. Kim, S. H. Yun, *Adv. Mater* **2015**, *27*, 4081.
[40] S. Tanosaki, H. Taniguchi, K. Tsujita, H. Inaba, *Appl. Phys. Lett.* **1996**, *69*, 719.
[41] J. R. Howell, M. P. Menguc, R. Siegel, *Thermal Radiation Heat Transfer*, CRC Press, Boca Raton, FL **2010**.
[42] P. Shorten, C. McMahon, T. Soboleva, *Biophys. J.* **2007**, *93*, 3001.